arXiv:2505.14359v1 [cs.CV] 20 May 2025

# Dual Data Alignment Makes AI-Generated Image Detector Easier Generalizable

**Ruoxin Chen**
Tencent YouTu Lab
cusmochen@tencent.com

**Junwei Xi**
East China University of Science and Technology
xjw@mail.ecust.edu.cn

**Zhiyuan Yan**
Peking University
yanzhiyuan1114@gmail.com

**Ke-Yue Zhang**
Tencent
zkyezhang@tencent.com

**Shuang Wu**
Tencent YouTu Lab
calvinwu@tencent.com

**Jingyi Xie**
Tsinghua University
jingyi_xie96@163.com

**Xu Chen**
East China University of Science and Technology
mejistus@outlook.com

**Lei Xu**
Shenzhen University
2022090123@email.szu.edu.cn

**Isabel Guan**
Hong Kong University of Science and Technology
eeguan@ust.hk

**Taiping Yao**
Tencent Youtu Lab
taipingyao@tencent.com

**Shouhong Ding**
Tencent Youtu Lab
ericshding@tencent.com

## Abstract

The rapid increase in AI-generated images (AIGIs) underscores the urgent need for generalizable detection methods. Existing detectors, however, are often trained on biased datasets, leading to the possibility of overfitting on non-causal image attributes that are spuriously correlated with real/synthetic labels. While these biased features enhance performance on the training data, they result in substantial performance degradation when applied to unbiased datasets. One common solution is to perform dataset alignment through generative reconstruction, matching the semantic content between real and synthetic images. However, we revisit this approach and show that pixel-level alignment alone is insufficient — the reconstructed images still suffer from frequency-level misalignment, which can perpetuate spurious correlations. To illustrate, we observe that reconstruction models tend to restore the high-frequency details lost in real images (possibly due to JPEG compression), inadvertently creating a frequency-level misalignment, where synthetic images appear to have richer high-frequency content than real ones. This misalignment leads to models associating high-frequency features with synthetic labels, further reinforcing biased cues. To resolve this, we propose Dual Data Alignment (DDA), which aligns both the pixel and frequency domains. DDA generates synthetic images that closely resemble real ones by fusing real and synthetic image pairs in both domains, enhancing the detector's ability to identify forgeries without

relying on biased features. Moreover, we introduce two new test sets: DDA-COCO, containing DDA-aligned synthetic images for testing detector performance on the most aligned dataset, and EvalGEN, featuring the latest generative models for assessing detectors under new generative architectures such as visual auto-regressive generators. Finally, our extensive evaluations demonstrate that a detector trained exclusively on DDA-aligned MSCOCO could improve across 8 diverse benchmarks by a non-trivial margin, showing a +7.2% on in-the-wild benchmarks, highlighting the improved generalizability of unbiased detectors.

## 1 Introduction

The rise of AI-generated images (AIGIs) poses significant risks to digital security, including the potential for misinformation, fraud, and copyright violations [11, 18, 19, 16, 28, 40, 38, 37]. This severe security issue underscores the urgent need for reliable detection methods to differentiate synthetic images from authentic ones. Despite advances in AIGI detection techniques [4, 26, 29], the rapid evolution of generative models and the emergence of new architectures present cross-domain generalization challenges. This is especially evident in zero-shot scenarios involving previously unseen generation paradigms.

The generalizability of AIGI detectors is hindered by dataset biases [12, 4, 27, 13]. Existing datasets often exhibit systematic discrepancies in attributes unrelated to the authority. Works [31] illustrate semantic bias through word frequency analysis, and studies [29] demonstrate image size bias by analyzing six datasets where synthetic images are uniformly sized as multiples of $128 \times 128$. These non-causal features could be exploited by models to distinguish real from synthetic images, resulting in biased detector performance that fails to generalize across different datasets. Figure 1 visually illustrates such bias. **Dataset alignment holds promise in addressing the issue of dataset bias** by ensuring synthetic images closely resemble real ones, *excluding authenticity-related factors* and *directing detectors to focus on forgery-related cues*. Specifically, studies [12] reveal systematic discrepancies in format and size biases: real images are JPEG-encoded and vary in size, whereas synthetic images are uniformly PNG-encoded and fixed in size. SemGIR [39], DRCT [4], B-Free [13] aim to mitigate content discrepancies using diffusion reconstruction techniques that generate images semantically similar to real ones. Works [14, 41] prevent models from learning semantics-dependent features by breaking images into patches and shuffling them. However, in this paper, we ask: *Does reconstruction truly eliminate the potential misalignment and bias?* Our answer is NO, as we found that although reconstruction-based methods align datasets at the pixel level, they still **introduce subtle misalignments at the frequency level**. Specifically, generative alignement methods, including generative reconstruction, provide detailed information across all frequency bands. In particular, the reconstructed images restore high-frequency components that are typically diminished in real images, possibly due to compression during transmission or storage. Consequently, **synthetic images exhibit prominent high-frequency details, while real images show only minor**, creating a noticeable disparity in the quantity of high-frequency components, rather than in the actual high-frequency content itself. This spurious correlation can cause the model learned to learn such a bias could mistakenly recognize.

In this paper, we propose **D**ual **D**ata **A**lignment (DDA), an effective technique that aligns synthetic images with real ones across both pixel and frequency domains. DDA consists of three steps: 1) VAE reconstruction for pixel alignment, 2) high-frequency fusion to eliminate bias, and 3) pixel mixup for further alignment in the pixel domain. As shown in Figure 2, **a single model trained on DDA-aligned MSCOCO demonstrates significant improvements across benchmarks: +12.4% on GenImage [1], +9.8% on Synthbuster and +17.7% on EvalGEN, with significantly lower fluctuations across subset evaluation performance – usually 1/3 to 2/3 that of the SoTA detectors – suggesting that DDA learns a reliable and general feature.** Moreover, we introduce two new evaluation datasets: 1. DDA-COCO, a test set consisting of real images from MS COCO and their DDA-aligned counterparts, which are mostly aligned. Evaluation results show that prior detectors suffer significant performance drops on DDA-COCO, further validating the alignment quality of the DDA method. 2. EvalGEN, a test set consisting of FLUX, GoT, Infinity, NOVA, and OmniGen, which

[1] In the test, we use JPEG-aligned GenImage, where synthetic images are compressed with a JPEG quality factor of 96, matching the format of real images. This approach helps mitigate format bias-based discrimination.

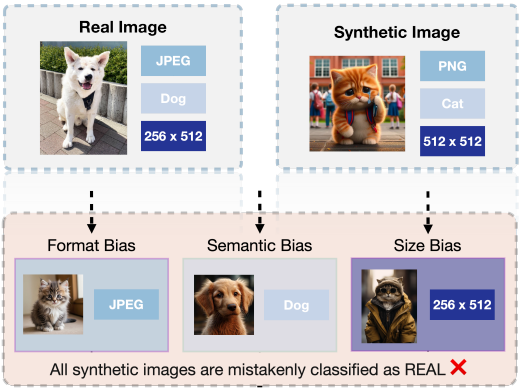


Figure 1: **Illustration of dataset bias.** Top row: Real and synthetic images may show disparities in format, content, and size. Real images are typically in JPEG format, with varying sizes and centered semantics. Bottom row: Detectors trained on datasets containing these discrepancies are prone to learning biased features, incorrectly associating authenticity with format, image size, or semantics. This leads to an inability to detect synthetic images that resemble real training data in specific characteristics.

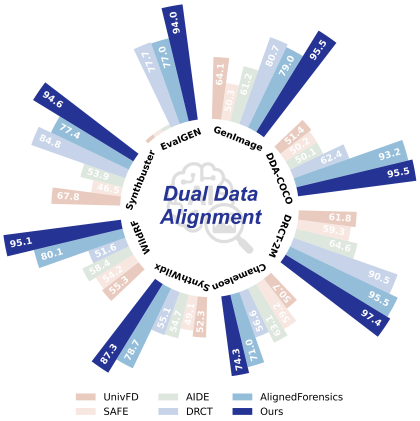


Figure 2: **Overall average balanced accuracy comparison between detection methods on eight different test sets.** Our model is exclusively trained on MSCOCO real images with DDA alignment. The consistent outperformance of DDA on three in-the-wild (Chameleon, WildRF, and SynthWildx) and five manually-crafted datasets validates the generalizability. Detailed settings and results are provided in Section 4, which also demonstrate that DDA exhibits lower cross-dataset performance fluctuations.

includes both advanced auto-regressive and diffusion generators, serving for measuring detectors' generalizability under newly evolved generative models.

## 2 Related Works

**AIGI Detection.** CNNSpot [34] trains a vanilla CNN model to detect AIGI, finding that detectors easily recognize synthetic images from seen models but struggle to generalize to unseen ones. UnivFD [26] employs CLIP as the detector backbone, showing the improvements in generalizability in detecting unseen generators with pretrained models. Subsequent works [25, 31, 41] explore model architectures and image preprocessing for more generalizable AIGI detection. C2P-CLIP enhances the pretrained CLIP backbone for AIGI detection by injecting 'real' and 'fake' concepts. Works [32, 5, 21, 17] exploit frequency domain artifacts, showing that frequency artifacts could well discriminate. NPR [33] explores the upsampling artifact in generative models. However, these methods' generalizability is limited by either content bias or frequency-level bias, with a significant chance of exploiting non-causal features like image format, which can significantly degrade performance on unbiased test sets.

**Dataset alignment.** The evaluation bias issue in AIGI detection is firstly introduced in the work [12], showing that image format and size are common biases unintentionally exploited by detectors. FakeInversion [3] introduces a bias-reduced evaluation benchmark, mitigating thematic and stylistic biases by collecting synthetic images that match real images in both content and style. A line of subsequent works explores eliminating bias in the training set to enhance generalizability. SemGIR [39] regenerates synthetic images by semantic-level reconstruction conditioned on the real counterpart's description, aiming to better align synthetic and real images semantically. DRCT [4] employs diffusion reconstruction for improved semantic alignment. B-Free [13] addresses dataset bias through self-conditioned inpainted reconstructions and content augmentation. However, this inpainting paradigm can alter the center object, corrupting the semantic alignment. AlignedForensics [27] performs simple VAE reconstruction without latent space manipulation, resulting in synthetic images that closely match real images in semantics and resolution. However, both B-Free and AlignedForensics overlook format alignment, creating space for JPEG-based shortcuts in discrimination. These methods are summarized in Table 1.

Table 1: Comparing on dataset alignment.

| Domaim | UnivFD [26] | C2P-CLIP [31] | SAFE [21] | AIDE [36] | DRCT [4] | AlignedForensics [27] | Ours |
|---|---|---|---|---|---|---|---|
| Frequency | Low | Low | Low | Low | Low | Low | High |
| Pixel | Low | Low | Low | Low | Medium | High | High |

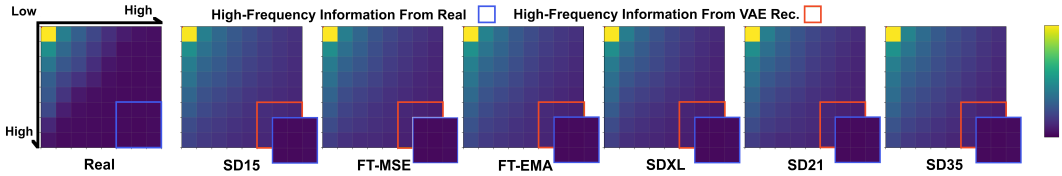


Figure 3: **Visualization of frequency domain energy using 2D Discrete Cosine Transform (DCT).** The left column shows a real image, while the remaining columns display images reconstructed by VAEs from various Stable Diffusion models. The grids represent frequency components, with the top-left and bottom-right indicating low- and high-frequency regions, respectively. Lighter areas correspond to higher energy. Notably, real images exhibit significantly darker high-frequency regions compared to VAE reconstructions, indicating weaker high-frequency content in real images and rich high-frequency signals in synthetic ones.

# 3 Methodology

## 3.1 Motivation and Analysis

**Misaligned Dataset.** Without additional supervision, detectors rely solely on the training set to learn the concept of 'real vs. synthetic'. When these two classes systematically differ in attributes like image size, style, or semantics, the model may mistakenly treat these non-causal disparities as defining characteristics of 'real' versus 'fake.' In particular, some of these discrepancies are particularly evident and easy for models to detect. However, genuine real-synthetic artifacts are subtle and often imperceptible, making them harder for detectors to learn the true unbiased features.

**Reconstruction-based alignment.** To align synthetic images with real ones, some approaches [39, 42, 13] employ txt2img generative models to generate images with similar semantic content, conditioned on the image label or image captions obtained through pretrained models. However, images generated using this approach often differ from the originals due to the lack of strong and detailed supervision, which prevents the generated images from fully matching the original images in all semantic details. DRCT [4, 13] leverages Img2Img diffusion reconstruction, directly using the image itself to guide the reconstruction of a real image $x$ into a synthetic counterpart $\hat{x}$ as follows:

$$\hat{x} = \text{Decoder}(\hat{z}), \quad \text{where} \quad \hat{z} = z + \epsilon_t - \epsilon_\theta(z, t), \quad z = \text{Encoder}(x) \tag{1}$$

where $z$ represents the encoded latent of the real image, while $\hat{z}$ is modified by adding noise and subsequently denoising, creating new latents that subtly differ from $z$.However, such self-supervised diffusion reconstruction can still lead to changes in image details due to modifications in the latent space, which is responsible for the generation of semantics. The work [27] further simplifies the reconstruction process by using a Variational Autoencoder (VAE)—a submodule used in all stable diffusion generators—without any modification to the latent. This approach generates images that

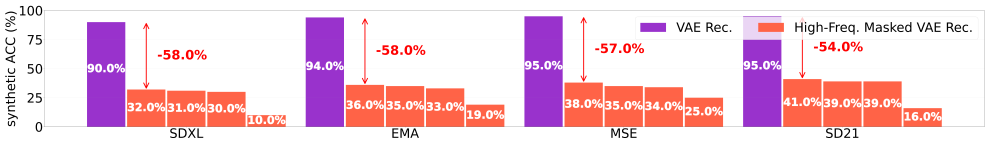


Figure 4: **Evidence for the existence of biased frequency-based features to discriminate reconstructed images.** We apply a binary mask to the DCT coefficients, systematically nullifying high-frequency components where either the horizontal or vertical frequencies exceed 95%, 90%, 85% and 80% of their respective spectral ranges to generate High-Freq. Masked VAE Rec.

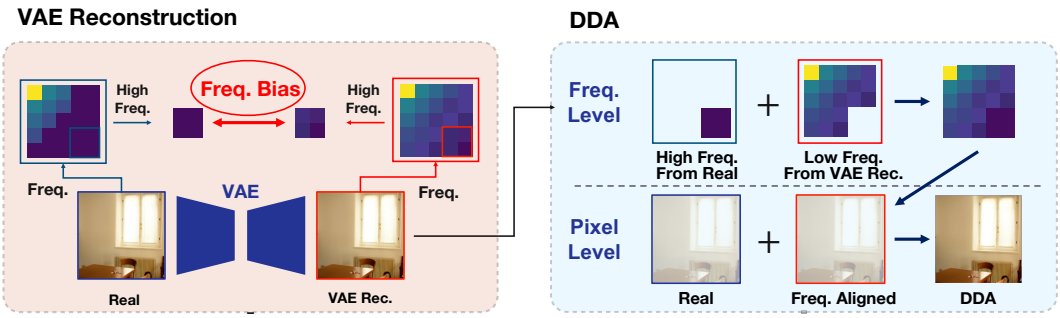


Figure 5: Illustration of DDA pipeline. **Left:** VAE-reconstructed images differ from real images in the intensity of high-frequency components. **Right:** DDA aligns images by first fusing high-frequency information from real images into the VAE-reconstructed images to align them in the frequency domain. Then, DDA uses pixel-level mixup of real and frequency-aligned images to further align them in the pixel domain.

closely match the original real image at the pixel level.

$$\hat{x} = \text{Decoder}(z), \quad \text{where} \quad z = \text{Encoder}(x) \tag{2}$$

**Frequency-Level Misalignment Exists and Can Be Exploited.** Frequency-domain analysis has been widely explored in AIGI detectors [30, 21, 24, 36], demonstrating that frequency information is a crucial feature for AIGI detection. This motivates us to revisit the alignment of synthetic images in the frequency domain. Surprisingly, despite pixel-level alignment, synthetic counterparts exhibit significant discrepancies in high-frequency content. Figure 3 visualizes this discrepancy between the real image and synthetic images reconstructed using various VAEs. Real images are often with relatively poor high-frequency information, which likely due to operations such as JPEG compression removing high-frequency details like sharp edges and fine textures, elements less noticeable to the human eye. Having identified this frequency-level discrepancy, another question arises: "Can this disparity be leveraged, or are we overestimating its impact?" To evaluate its effect, we assess the impact of high-frequency information by measuring the variance in detector performance on VAE-reconstructed images. As shown in Figure 4, the empirical results are surprising: visually identical VAE-reconstructed images are easily detected by the frequency-based SAFE detector [21], with a detection rate of 93%, suggesting an evident difference in the frequency domain. However, when we mask high-frequency information minorly, the detection rate significantly drops. This substantial drop is unlikely to be solely attributed to information loss, but rather suggests that detectors may be exploiting biased features, specifically the presence of richer high-frequency details in synthetic images. In conclusion, we expose the frequency-level discrepancy between real and synthetic images, demonstrating that this misalignment can be exploited by certain detectors.

### 3.2 Dual Data Alignment

Motivated by the previous observation, we propose DDA, a technique that generates synthetic images aligned with real ones in both the pixel and frequency domains to mitigate the learning of biased features. As illustrated in Figure 5, DDA consists of three steps: 1) **VAE Reconstruction:** Generate pixel-wise similar images containing VAE-specific artifacts. 2) **Frequency-Level Alignment:** Fuse high-frequency components from real images into the VAE-reconstructed images to eliminate discrepancies in the frequency domain. Specifically, we replace the 2D-DCT coefficients whose horizontal or vertical frequencies exceed a predefined threshold $T_{freq}$ with those from the corresponding real image. 3) **Pixel-Level Alignment:** Apply mixup between real and frequency-aligned images to ensure pixel-domain alignment. Concretely, we generate a closely aligned synthetic image as follow:

$$x_{\text{mix}} = r_{pixel} \cdot x_{real} + (1 - r_{pixel}) \cdot x_{syn} \tag{3}$$

where $r_{pixel} \in [0, 1]$ controls the degree of pixel-level alignment. A higher $r_{pixel}$ value yields a closer synthetic image in the pixel space. In practice, $r_{pixel}$ is sampled from a uniform distribution $\mathcal{U}(0, R_{pixel})$. A higher $r_{pixel}$ value results in a synthetic image that more closely resembles the real image in pixel space. Together, these steps ensure that the resulting synthetic images preserve generative artifacts while maintaining close alignment with real data, both spectrally and spatially—guiding the model to learn meaningful rather than spurious features.

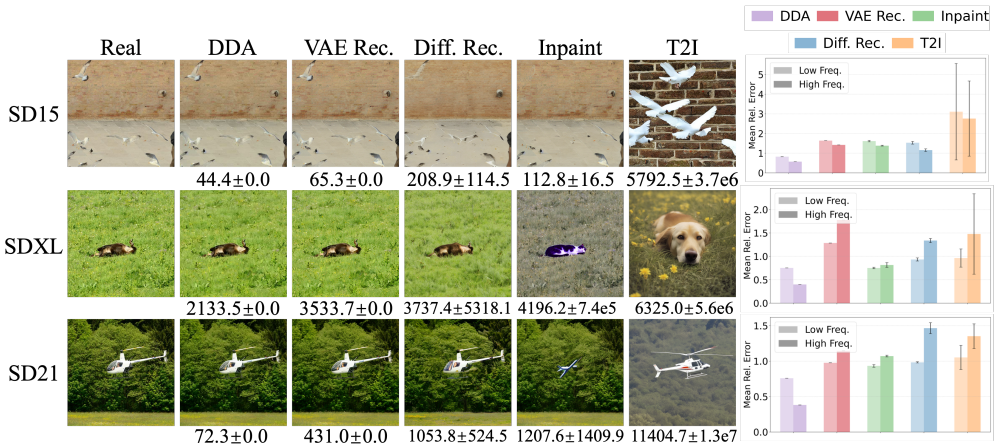


Figure 6: Comparison of various image processing methods based on loss with respect to the real image. **Left:** Comparison of image processing methods across three Stable Diffusion model series (SD15, SDXL, SD21) displaying real images alongside processed versions using DDA, VAE reconstruction (VAE Rec.), diffusion reconstruction (Diff. Rec.), masked inpainting with prompts (Inpaint), and text-to-image generation (T2I). Mean squared error (MSE) values relative to the real image are presented beneath each processed image, and each mse value is calculated by generating 100 images. **Right:** Visualization of relative error metrics for each processing method across the same model series, segregated into low frequency and high frequency bands as calculated using discrete Fourier transform (DFT). Bar charts illustrate comparative error magnitudes across different reconstruction techniques and frequency components. Both pixel-level and frequency-level analyses indicate that DDA produces synthetic images most similar to the real images.

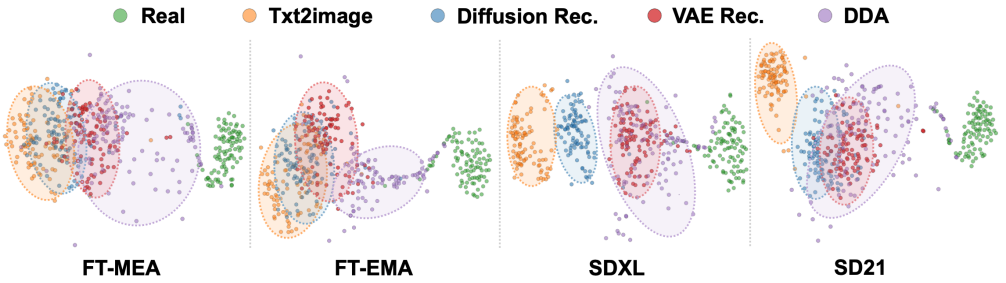


Figure 7: t-SNE visualizations comparing real and generated images, illustrating the proximity of synthetic image cluster centers to real images in feature space. The ordering of proximity—from closest to farthest—is: DDA, VAE reconstruction, diffusion reconstruction, and text-to-image (T2I) generation. These results indicate that DDA produces synthetic samples most closely aligned with real images near the data manifold boundary, thereby facilitating the learning of a tighter and more generalizable decision boundary.

The generalizability of DDA is built upon two foundations: 1) **VAE artifacts generalize across generators.** Because VAE-reconstructed images are the closest synthetic counterparts to real images, decision boundaries learned from these pairs are likely to remain effective for distinguishing other, more distant synthetic variants (e.g., those from text-to-image generators). Moreover, since the VAE decoder is typically the final stage in diffusion-based generators, its artifacts are less influenced by subsequent modules. 2) **Dual-domain alignment mitigates dataset bias.** By aligning synthetic images with real ones in both the frequency and pixel domains, DDA reduces real-synthetic discrepancies more effectively than alternative reconstruction-based methods. In particular, it eliminates high-frequency bias—commonly introduced by compression or generative artifacts—leading to stronger generalization and reduced reliance on spurious features.

**Comparison to Dataset Alignment Methods.** We validate that DDA creates the closest real-synthetic image pairs when compared to other alignment methods from the following three viewpoints: 1) Pixel domain: Left of Figure 6 shows that DDA-aligned images lead to minimal MSE loss compared to the original image; 2) Frequency domain: Right of Figure 6 shows that DDA-aligned images are

most similar to the original image in frequency space; 3) Feature domain: Figure 7 validates that the cluster center of DDA-aligned images is closest to the center of real images.

# 4 Experiments

## 4.1 Experimental Setup

**Datasets** All compared detectors are evaluated on eight diverse datasets, including four benchmark datasets (GenImage [42], DRCT-2M [4], EvalGEN, and Synthbuster [1]) and three in-the-wild datasets (Chameleon [36], WildRF [2], and SynthWildx [6]), where images are sourced from the web. These datasets contain real images from different sources and various generators, including diffusion models, GAN models, auto-regressive models, and other unknown models. They differ in format, content, and resolution, thereby minimizing evaluation bias. Table 2 outlines the datasets' details.

**DDA-COCO and EvalGEN** DDA-COCO consists of five subsets containing reconstructed images of MSCOCO [22] validation set by different VAEs, utilizing frequency-level alignment. We construct the EvalGEN dataset using the five latest text-to-image (T2I) generators using aligned prompts from the GenEval benchmark [10]. Notably, **we are the first work to involve auto-regressive-based T2I generators for image forensics** in the AIGI detection field. Specifically, we introduce each generator as follows: (1) **Flux** [20]: the SOTA diffusion-based generator, offering extremely higher-resolution output images. (2) **GoT** [9]: A multimodal model combining LLM and diffusion processes to enable reasoning-guided image generation. (3) **Infinity** [15]: A bitwise auto-regressive model using infinite-vocabulary tokenization and self-correction for faster and higher-fidelity image generation. (4) **OmiGen** [35]: A unified multimodal framework capable of handling diverse image generation tasks within a single, simplified architecture. (5) **NOVA** [8]: A non-quantized auto-regressive model designed for efficient image and video generation, achieving high fidelity with reduced computational overhead. These models allow our **EvalGEN to serve as a very high-quality benchmark** for evaluating the generalizability of detectors on unseen generators.

**Implementation Details** We utilize DINOv2 as the backbone and fine-tune it using LoRA with a rank of 8. The input size is set to 336×336, using random cropping during training and center cropping during validation. Padding is applied when the image height or width is insufficient. The training data exclusively consists of MSCOCO [23] images and their DDA-aligned counterparts. All evaluations of DDA are performed using a single model, without any dataset-specific fine-tuning. More implementation details are omitted into Appendix due to space constraint.

**Evaluation Metrics and Comparative Methods** Unless otherwise specified, we report balanced accuracy, defined as the average of real and fake class accuracies, following the mainstream line of works [7, 26, 25, 21, 31, 36, 4, 27, 13], to evaluate the effectiveness and generalizability of detection methods. The compared methods include four frequecy-based detectors: NPR [7], SAFE [21] and AIDE [36], three CLIP-based detectors: UnivFD [26], Fatformer [25] and C2P-CLIP [31] and two data alignment methods: DRCT [4] and AlignedForensics [27]. For fairness and reproducibility, we use publicly released checkpoints from the official GitHub repositories of these methods. [2]

## 4.2 Cross-Dataset Comparison

**Comparison on DDA-COCO** Table 3 reports real and fake accuracy scores on our proposed DDA-COCO. We observe the following: (1) Our method, trained solely on SD 2.1 reconstructed data, generalizes well to other diffusion models—surpassing the second-best by 7.7% in fake accuracy—and exhibits a smaller standard deviation than second-best detector. This suggests the model has learned a universal upsampling artifact present across diverse generative models, supporting the claim that better data alignment improves generalizability. We hypothesize that this artifact arises during the VAE-based decoding process (2) Furthermore, the DDA-COCO results highlight the importance of data alignment. Methods lacking alignment—such as NPR [7], UnivFD [26], FatFormer [25], C2P-CLIP [31], AIDE [36], and SAFE [21]—show large disparities between real and fake accuracy, revealing biases related to format, content, or resolution, as discussed in [31, 41]. AlignedForensics [27], which applies partial alignment (format & content), achieves higher performance—86.6% fake accuracy—further confirming alignment's effectiveness.

[2] B-Free [13] is excluded from comparison except WildRF due to the lack of publicly available code and insufficient experimental reporting from original paper, which makes faithful reproduction prohibitively expensive and unreliable. For WildRF, we use the reported results from the original paper.

Table 2: Datasets Overview. "SD" is stable diffusion and "AR" is auto-regressive model.

| Dataset | Real / Fake | Source | # Models | Model Types |
|---|---|---|---|---|
| DDA-COCO | 5K / 30K | MSCOCO | 6 | SD |
| GenImage [42] | 48K / 48K | ImageNet | 8 | SD & GAN |
| DRCT-2M [4] | 5K / 80K | MSCOCO | 16 | SD |
| Synthbuster [1] | 1K / 9K | RAISE | 9 | SD & AR |
| EvalGEN | 0 / 55.3K | Prompt | 7 | SD & AR |
| Chameleon [36] | 14.9K / 11.2K | Internet | unknown | unknown |
| WildRF [2] | 500 / 500 | Reddit, FB, X | unknown | unknown |
| SynthWildx [6] | 500 / 1.5K | X | 3 | SD & AR |

Table 3: Comparison on DDA-COCO.

| Method | real | fake | | | | | |
|---|---|---|---|---|---|---|---|
| | | XL | EMA | MSE | SD21 | SD35 | Avg. |
| NPR (ECCV'24) [7] | 55.4 | 21.0 | 31.0 | 29.8 | 29.1 | 29.6 | 28.1 ± 4.0 |
| UnivFD (CVPR'23) [26] | <u>99.2</u> | 2.7 | 5.3 | 3.8 | 4.3 | 1.9 | 3.6 ± 1.3 |
| FatFormer (CVPR'24) [25] | 96.4 | 2.3 | 3.1 | 4.2 | 4.3 | 2.4 | 3.3 ± 0.9 |
| SAFE (KDD'25) [21] | 98.8 | 0.5 | 0.6 | 0.5 | 0.4 | 0.3 | 0.5 ± 0.1 |
| C2P-CLIP (AAAI'25) [31] | 99.5 | 1.6 | 1.7 | 2.2 | 2.2 | 2.3 | 2.0 ± 0.3 |
| AIDE (ICLR'25) [36] | 98.8 | 1.1 | 2.2 | 0.9 | 0.8 | 1.0 | 1.2 ± 0.6 |
| DRCT (ICML'24) [4] | 94.2 | 24.5 | 34.7 | 33.1 | 33.6 | 26.3 | 30.4 ± 4.7 |
| AlignedForensics (ICLR'25) [27] | **99.8** | 82.5 | <u>99.3</u> | <u>99.0</u> | 99.0 | 53.2 | 86.6 ± 20.0 |
| VAE Rec. | 94.4 | <u>94.3</u> | 96.2 | 96.3 | 96.6 | <u>66.4</u> | <u>90.0</u> ± 12.2 |
| **VAE Rec. + DDA (ours)** | 96.8 | **98.3** | **99.7** | **99.9** | **99.8** | **73.9** | **94.3** ± 11.4 |

Table 4: Performance comparison on the DRCT-2M benchmark. "VAE Rec." denotes training with SD21 VAE-reconstructed images using the same architecture and training settings as our method, but without Dual Data Alignment (DDA). "VAE Rec. + DDA (ours)" represents our full approach, applying DDA on top of the VAE-reconstructed training set. Bold numbers indicate the best performance per column; underlined numbers indicate the second-best.

| Method | LDM | SDv1.4 | SDv1.5 | SDv2 | SDXL | SDXL-Refiner | SD-Turbo | SDXL-Turbo | LCM-SDv1.5 | LCM-SDXL | SDv1-Ctrl | SDv2-Ctrl | SDXL-Ctrl | SDv1-DR | SDv2-DR | SDXL-DR | Avg. |
|---|---|---|---|---|---|---|---|---|---|---|---|---|---|---|---|---|---|
| NPR (ECCV'24) [7] | 33.0 | 29.1 | 29.0 | 35.1 | 33.2 | 28.4 | 27.9 | 27.9 | 29.4 | 30.2 | 28.4 | 28.3 | 34.7 | 67.9 | 67.4 | 66.1 | 37.3 ± 15.0 |
| UnivFD (CVPR'23) [26] | 85.4 | 56.8 | 56.4 | 58.2 | 63.2 | 55.0 | 56.5 | 53.0 | 54.5 | 65.9 | 68.0 | 65.4 | 75.9 | 64.6 | 56.2 | 53.9 | 61.8 ± 8.9 |
| FatFormer (CVPR'24) [25] | 55.9 | 48.2 | 48.2 | 48.2 | 48.2 | 48.3 | 48.2 | 48.2 | 48.3 | 50.6 | 49.7 | 49.9 | 59.8 | 66.3 | 60.6 | 56.0 | 52.2 ± 5.7 |
| SAFE (KDD'25) [21] | 50.3 | 50.1 | 50.0 | 50.0 | 49.9 | 50.1 | 50.0 | 50.0 | 50.1 | 50.0 | 49.9 | 50.0 | 54.7 | 98.2 | 98.5 | 97.3 | 59.3 ± 19.2 |
| C2P-CLIP (AAAI'25) [31] | 83.0 | 51.7 | 51.7 | 52.9 | 51.9 | 64.6 | 51.7 | 50.6 | 52.0 | 66.1 | 56.9 | 54.7 | 77.8 | 67.2 | 57.1 | 56.7 | 59.2 ± 9.9 |
| AIDE (ICLR'25) [36] | 64.4 | 74.9 | 75.1 | 58.5 | 53.5 | 66.3 | 52.8 | 52.8 | 70.0 | 54.3 | 65.9 | 53.6 | 53.9 | 95.3 | 73.3 | 69.0 | 64.6 ± 11.8 |
| DRCT (ICML'24) [4] | 96.7 | 96.3 | 96.3 | 94.9 | **96.2** | 93.5 | 93.4 | <u>92.9</u> | 91.2 | 95.0 | 95.6 | 92.7 | 92.0 | 94.1 | 69.6 | 57.4 | 90.5 ± 7.4 |
| AlignedForensics (ICLR'25) [27] | **99.9** | **99.9** | **99.9** | **99.6** | 90.2 | 81.3 | **99.7** | 89.4 | **99.7** | 90.0 | **99.9** | **99.2** | 87.6 | **99.9** | **99.8** | 92.6 | 95.5 ± 6.1 |
| VAE Rec. | 97.5 | 96.5 | 95.8 | 96.4 | <u>95.2</u> | <u>94.1</u> | 93.4 | 91.9 | 93.9 | <u>96.8</u> | 96.9 | 97.1 | <u>97.4</u> | 97.3 | 97.5 | <u>95.5</u> | <u>95.8</u> ± 1.7 |
| **VAE Rec. + DDA (ours)** | <u>98.4</u> | <u>98.1</u> | <u>97.8</u> | <u>97.5</u> | **96.2** | **96.3** | <u>96.6</u> | **95.4** | <u>97.5</u> | **97.9** | <u>98.2</u> | <u>98.2</u> | **98.4** | <u>98.1</u> | <u>98.4</u> | **96.2** | **97.4** ± 1.2 |

Table 5: Comparison on GenImage.

| Method | Midjourney | SDv1.4 | SDv1.5 | ADM | GLIDE | Wukong | VQDM | BigGAN | Avg. |
|---|---|---|---|---|---|---|---|---|---|
| NPR (ECCV'24) [7] | 53.4 | 55.1 | 55.0 | 43.8 | 41.2 | 57.4 | 48.4 | 57.7 | 51.5 ± 6.3 |
| UnivFD (CVPR'23) [26] | 55.1 | 55.6 | 55.7 | 62.5 | 61.3 | 61.1 | 76.9 | 84.4 | 64.1 ± 10.8 |
| FatFormer (CVPR'24) [25] | 52.1 | 53.6 | 53.8 | 61.4 | 65.5 | 60.9 | 72.5 | 82.2 | 62.8 ± 10.4 |
| SAFE (KDD'25) [21] | 49.0 | 49.7 | 49.8 | 49.5 | 53.0 | 50.3 | 50.2 | 50.9 | 50.3 ± 1.2 |
| C2P-CLIP (AAAI'25) [31] | 56.6 | 77.5 | 76.9 | 71.6 | 73.5 | 79.4 | 73.7 | 85.9 | 74.4 ± 8.4 |
| AIDE (ICLR'25) [36] | 58.2 | 77.2 | 77.4 | 50.4 | 54.6 | 70.5 | 50.8 | 50.6 | 61.2 ± 11.9 |
| DRCT (ICML'24) [4] | 82.4 | 88.3 | 88.2 | 76.9 | <u>86.1</u> | 87.9 | <u>85.4</u> | 87.0 | 84.7 ± 2.7 |
| AlignedForensics (ICLR'25) [27] | **97.5** | **99.7** | **99.6** | 52.4 | 57.6 | **99.6** | 75.0 | 50.6 | 79.0 ± 22.7 |
| VAE Rec. | 87.1 | 91.0 | 89.7 | <u>82.7</u> | 74.7 | 90.7 | 84.2 | <u>89.4</u> | <u>86.2</u> ± 5.2 |
| **VAE Rec. + DDA (ours)** | <u>94.4</u> | <u>97.3</u> | <u>97.2</u> | **94.3** | **93.1** | <u>97.3</u> | **94.6** | **95.8** | **95.5** ± 1.6 |

Table 6: Comparison on EvalGEN.

| Method | Flux | GoT | Infinity | OmiGen | NOVA | Avg. |
|---|---|---|---|---|---|---|
| NPR (ECCV'24) [7] | 52.0 | 41.6 | 77.2 | 64.2 | 61.2 | 59.2 ± 2.0 |
| UnivFD (CVPR'23) [26] | 4.0 | 9.2 | 15.7 | 8.3 | 39.6 | 15.4 ± 0.7 |
| FatFormer (CVPR'24) [25] | 9.9 | 47.8 | 44.7 | 98.3 | 27.3 | 45.6 ± 33.1 |
| SAFE (KDD'25) [21] | 1.0 | 0.5 | 1.9 | 0.6 | 1.6 | 1.1 ± 0.1 |
| C2P-CLIP (AAAI'25) [31] | 8.7 | 49.4 | 35.1 | 86.4 | 14.8 | 38.9 ± 31.1 |
| AIDE (ICLR'25) [36] | 16.2 | 21.6 | 4.0 | 14.9 | 18.4 | 15.0 ± 6.7 |
| DRCT (ICML'24) [4] | <u>72.2</u> | 81.4 | 77.8 | 84.8 | 72.5 | 77.7 ± 5.5 |
| AlignedForensics (ICLR'25) [27] | 45.0 | 84.4 | 79.6 | <u>90.8</u> | 85.2 | 77.0 ± 18.3 |
| VAE Rec. | 64.0 | <u>89.6</u> | <u>88.2</u> | 88.6 | <u>89.7</u> | <u>84.2</u> ± 11.3 |
| **VAE Rec. + DDA (ours)** | **87.0** | **99.3** | **99.5** | **99.5** | **100.0** | **94.0** ± 5.6 |

Table 7: Comparison on Synthbuster.

| Method | DALL-E 2 | DALL-E 3 | Firefly | GLIDE | Midjourney | SD 1.3 | SD 1.4 | SD 2 | SDXL | Avg. |
|---|---|---|---|---|---|---|---|---|---|---|
| NPR (ECCV'24) [7] | 51.1 | 49.3 | 46.5 | 48.5 | 52.8 | 51.4 | 51.8 | 46.0 | 52.8 | 50.0 ± 2.6 |
| UnivFD (CVPR'23) [26] | 83.5 | 47.4 | 89.9 | 53.3 | 52.5 | 70.4 | 69.9 | 75.7 | 68.0 | 67.8 ± 14.4 |
| FatFormer (CVPR'24) [25] | 59.4 | 39.5 | 60.3 | 72.7 | 44.4 | 53.7 | 54.0 | 52.3 | 69.1 | 56.1 ± 10.7 |
| SAFE (KDD'25) [21] | 58.0 | 9.9 | 10.3 | 52.2 | 56.7 | 59.4 | 59.1 | 53.0 | 59.5 | 46.5 ± 20.8 |
| C2P-CLIP (AAAI'25) [31] | 55.6 | 63.2 | 59.5 | <u>86.7</u> | 52.9 | 75.2 | 76.7 | 69.2 | 77.7 | 68.5 ± 11.4 |
| AIDE (ICLR'25) [36] | 34.9 | 33.7 | 24.8 | 65.0 | 57.5 | 74.1 | 73.7 | 53.2 | 68.4 | 53.9 ± 18.6 |
| DRCT (ICML'24) [4] | 77.2 | <u>86.6</u> | 84.1 | 82.6 | 73.7 | 86.6 | 86.6 | 83.2 | 71.3 | 84.8 ± 3.6 |
| AlignedForensics (ICLR'25) [27] | 50.2 | 48.9 | 51.7 | 53.5 | **98.7** | **98.8** | **98.8** | **98.6** | **97.3** | 77.4 ± 25.0 |
| VAE Rec. | <u>86.0</u> | 86.1 | <u>85.8</u> | 78.1 | 86.1 | 86.0 | 86.1 | 86.0 | 86.3 | <u>85.2</u> ± 2.7 |
| **VAE Rec. + DDA (ours)** | **95.3** | **95.2** | **95.4** | **88.9** | <u>95.5</u> | <u>95.4</u> | <u>95.5</u> | <u>95.4</u> | <u>95.5</u> | **94.6** ± 2.2 |

Table 8: Comparison on Chameleon, SynthWildx.

| Method | Chameleon | SynthWildx | | | |
|---|---|---|---|---|---|
| | | DALL-E 3 | Firefly | Midjourney | Avg. |
| NPR (ECCV'24) [7] | 59.9 | 43.6 | 61.3 | 44.5 | 49.8 ± 10.0 |
| UnivFD (CVPR'23) [26] | 50.7 | 45.4 | 65.3 | 46.2 | 52.3 ± 11.3 |
| FatFormer (CVPR'24) [25] | 51.2 | 46.5 | 61.6 | 48.3 | 52.1 ± 8.2 |
| SAFE (KDD'25) [21] | 59.2 | 49.4 | 48.2 | 49.6 | 49.1 ± 0.7 |
| C2P-CLIP (AAAI'25) [31] | 51.1 | 56.9 | 61.4 | 53.0 | 57.1 ± 4.2 |
| AIDE (ICLR'25) [36] | 63.1 | 63.4 | 48.8 | 51.9 | 48.8 ± 0.8 |
| DRCT (ICML'24) [4] | 56.6 | 58.3 | 56.4 | 50.5 | 55.1 ± 1.8 |
| AlignedForensics (ICLR'25) [27] | <u>71.0</u> | <u>85.5</u> | 58.5 | **92.2** | 78.8 ± 17.8 |
| VAE Rec. | 62.8 | 82.4 | <u>81.7</u> | 81.4 | <u>77.1</u> ± 9.5 |
| **VAE Rec. + DDA (ours)** | **74.3** | **88.0** | **86.3** | <u>87.5</u> | **84.0** ± 6.5 |

Table 9: Comparison on WildRF.

| Method | Facebook | Reddit | Twitter | Avg. |
|---|---|---|---|---|
| NPR (ECCV'24) [7] | 78.1 | 61.0 | 51.3 | 63.5 ± 13.6 |
| UnivFD (CVPR'23) [26] | 49.1 | 60.2 | 56.5 | 55.3 ± 5.7 |
| FatFormer (CVPR'24) [25] | 54.1 | 68.1 | 54.4 | 58.9 ± 8.0 |
| SAFE (KDD'25) [21] | 50.9 | 74.1 | 37.5 | 57.2 ± 18.5 |
| C2P-CLIP (AAAI'25) [31] | 54.4 | 68.4 | 55.9 | 59.6 ± 7.7 |
| AIDE (ICLR'25) [36] | 57.8 | 71.5 | 45.8 | 58.4 ± 12.9 |
| DRCT (ICML'24) [4] | 46.6 | 53.1 | 55.2 | 50.6 ± 3.5 |
| AlignedForensics (ICLR'25) [27] | <u>89.4</u> | 69.1 | 81.8 | 80.1 ± 10.3 |
| B-Free (CVPR'24) [13] | **95.6** | 86.2 | **97.3** | <u>93.3</u> ± 9.4 |
| VAE Rec. | 89.5 | <u>91.8</u> | 93.5 | 88.3 ± 2.1 |
| **VAE Rec. + DDA (ours)** | 94.4 | **94.3** | <u>96.8</u> | **95.1** ± 1.4 |

**Comparison on DRCT-2M, GenImage and Synthbuster** Tables 4, 5, and 7 summarize comparisons on DRCT-2M, GenImage, and Synthbuster, respectively. We observe the following: (1) Our method outperforms the second-best approach by 1.9%, 10.8%, and 9.8% on the three datasets. Given the diversity of real image sources and the inclusion of both GAN- and diffusion-based models, these results strongly support the effectiveness and generalizability of our method. (2)Consistent with observations on DDA-COCO,detectors trained with better-aligned data consistently achieve higher accuracy. This reinforces the importance of proper alignment. Notably, DDA consistently outperforms the VAE Rec. baseline by a non-trivial margin across all benchmarks, underscoring the critical contribution of dual-domain alignment in enhancing detection robustness.

**Comparison on EvalGEN** Table 6 presents the balanced accuracy on the EvalGEN dataset. Our method surpasses the second-best approach by 14.8%, demonstrating strong generalizability. This superior performance on new generators supports the effectiveness and robustness of our detector. Among the models in EvalGEN, FLUX poses the greatest challenge due to the high realism of its generated images. While our method performs relatively lower on FLUX compared to other models, it still significantly outperforms the second-best approach by 8.6%.

Table 10: Comparing on data generation time.

| Method | # Real / Fake | Generation Method | Time Per Image | Full Construction Time |
|---|---|---|---|---|
| DRCT | 11.8K / 35.4K | Diff. Rec. | 0.6569 ± 0.0050 s | 6.46 h |
| AlignedForensics | 179K / 179K | VAE Rec. | 0.1756 ± 0.0692 s | 8.73 h |
| B-Free | 51K / 309K | Diff. Rec + Inpaint. | 3.0150 ± 0.0125 s | 258.79 h |
| **VAE Rec. + DDA (ours)** | 11.8K / 11.8K | VAE Rec. + DDA | 0.1792 ± 0.0704 s | 0.59 h |

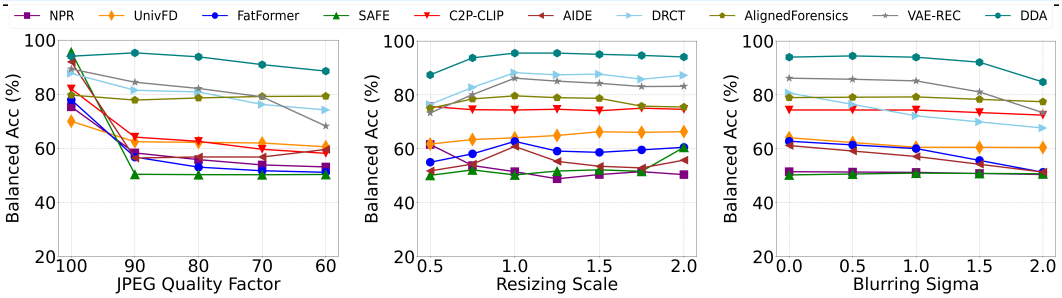


Figure 8: Robustness analysis on GenImage.

**Comparison on In-the-wild Datasets** Tables 8 and 9 demonstrate the balanced accuracy across three in-the-wild datasets. Our WildRF evaluation adopts the inference settings of B-Free [13]. We observe that: (1) Our method outperforms the second-best performing approach by 3.3%, 5.2% and 1.8% on Chameleon, SynthWildX and WildRF, while maintaining a relatively low standard deviation, indicating effectiveness and robustness in real-world scenarios. (2) To investigate the notably poor performance across detectors on the Chameleon dataset, we analyze its real images and identify widespread post-processing artifacts. These artifacts likely imped the detection of synthetic patterns.

**Comparison on Generation Time Cost** We compare three methods which introduce train data generation—DRCT [4], AlignedForensics [27], and B-Free [13]. Table 10 presents the number of real and fake images used for training, generation method and the estimated reconstruction time (Single Image & Full Set) using each method, which is tested by generating 100 synthetic images. Results show that our DDA requires the least amount of training data and reconstruction time, confirming its effectiveness and efficiency in terms of training cost.

### 4.3 Evaluation on Robustness

Figure 8 shows the results of three robustness evaluations on the GenImage-JPEG96 dataset for all compared methods. Results show that: (1) DDA shows strong robustness across all three post-processing methods, outperforming the second-best method by 9.3%, 6.8%, and 7.3% under JPEG 60, RESIZE 2.0, and BLUR 2.0, respectively. (2) Methods lacking alignment, such as NPR [7], SAFE [21], and AIDE [36], demonstrate poor robustness under JPEG compression and resizing. In contrast, methods with alignment like DRCT [4] and AlignedForensics [27] perform better, emphasizing the importance of data alignment. (3) All detectors are less robust to downsampling than upsampling, which we argue that the former irreversibly discards image details while the latter preserves the original content.

### 4.4 Ablation Studies

Figure 9 illustrates the impact of $T_{freq}$, $P_{pixel}$, $R_{pixel}$, and the choice of VAE in training data generation. Results indicate that a $T_{freq}$ value of 0.5 yields the best performance. The detector maintains consistent accuracy when $P_{pixel}$ and $R_{pixel}$ are between 0.2 and 0.8, with performance drops observed at 0.0 and 1.0, confirming the effectiveness of pixel-level alignment. Experiments with different VAEs confirm that SD21 is the most effective choice for training data generation.

## 5 Conclusion

In this paper, we first reveal that single reconstruction is insufficient for fully aligning real and synthetic image pairs. Building on this insight, we propose DDA to align synthetic images with real ones across pixel and frequency domains, thereby mitigating bias in AIGI detectors. We also introduce two AIGI datasets. DDA-COCO and EvalGEN. Extensive experiments on eight datasets demonstrate that our method outperforms state-of-the-art baselines by a margin of 7.5% on in-the-wild benchmark . We believe that DDA, DDA-COCO, and EvalGEN form a solid foundation for advancing the effectiveness and generalization of the whole AIGI detection field.

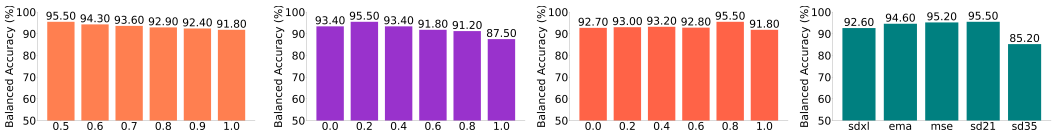


(a) Impact of $T_{freq}$ (b) Impact of $P_{pixel}$ (c) Impact of $r_{pixel}$ (d) Impact of VAE

Figure 9: **Ablation studies.** (a) $T_{freq}$: frequency threshold for frequency-level alignment; (b) $P_{pixel}$: probability of applying pixel-level alignment; (c) $R_{pixel}$: upper bound for sampling the pixel mixup ratio; (d) VAE: backbone used for training data reconstruction. Results show the impact of each hyperparameter on the performance of DDA.

**Limitations and Future Work** While our method demonstrates superior performance on both benchmark datasets and real-world scenarios, it may struggle to detect images with strong post-processing artifacts, as shown in the results on the Chameleon dataset. In future work, we plan to extend DDA to synthetic videos to enhance generalization in AI-generated video detection.

## References


[1] Q. Bammey. Synthbuster: Towards detection of diffusion model generated images. *IEEE Open Journal of Signal Processing*, 5:1–9, 2023.

[2] B. Cavia, E. Horwitz, T. Reiss, and Y. Hoshen. Real-time deepfake detection in the real-world. *arXiv preprint arXiv:2406.09398*, 2024.

[3] G. Cazenavette, A. Sud, T. Leung, and B. Usman. Fakeinversion: Learning to detect images from unseen text-to-image models by inverting stable diffusion. In *Proceedings of the IEEE/CVF Conference on Computer Vision and Pattern Recognition*, pages 10759–10769, 2024.

[4] B. Chen, J. Zeng, J. Yang, and R. Yang. Drct: Diffusion reconstruction contrastive training towards universal detection of diffusion generated images. In *Forty-first International Conference on Machine Learning*, 2024.

[5] B. Chu, X. Xu, X. Wang, Y. Zhang, W. You, and L. Zhou. Fire: Robust detection of diffusion-generated images via frequency-guided reconstruction error. In *CVPR*, 2025.

[6] D. Cozzolino, G. Poggi, R. Corvi, M. Nießner, and L. Verdoliva. Raising the bar of ai-generated image detection with clip. In *Proceedings of the IEEE/CVF Conference on Computer Vision and Pattern Recognition*, pages 4356–4366, 2024.

[7] D. Cozzolino, G. Poggi, M. Nießner, and L. Verdoliva. Zero-shot detection of ai-generated images. In *European Conference on Computer Vision*, pages 54–72. Springer, 2024.

[8] H. Deng, T. Pan, H. Diao, Z. Luo, Y. Cui, H. Lu, S. Shan, Y. Qi, and X. Wang. Autoregressive video generation without vector quantization. *arXiv preprint arXiv:2412.14169*, 2024.

[9] R. Fang, C. Duan, K. Wang, L. Huang, H. Li, S. Yan, H. Tian, X. Zeng, R. Zhao, J. Dai, et al. Got: Unleashing reasoning capability of multimodal large language model for visual generation and editing. *arXiv preprint arXiv:2503.10639*, 2025.

[10] D. Ghosh, H. Hajishirzi, and L. Schmidt. Geneval: An object-focused framework for evaluating text-to-image alignment. *Advances in Neural Information Processing Systems*, 36:52132–52152, 2023.

[11] I. J. Goodfellow et al. Generative adversarial nets. In *Advances in Neural Information Processing Systems*, 2014.

[12] P. Grommelt, L. Weiss, F.-J. Pfreundt, and J. Keuper. Fake or jpeg? revealing common biases in generated image detection datasets. *arXiv preprint arXiv:2403.17608*, 2024.

[13] F. Guillaro, G. Zingarini, B. Usman, A. Sud, D. Cozzolino, and L. Verdoliva. A bias-free training paradigm for more general ai-generated image detection. *arXiv preprint arXiv:2412.17671*, 2024.

[14] S. Gye, J. Ko, H. Shon, M. Kwon, and J. Kim. Sfld: Reducing the content bias for ai-generated image detection. *arXiv preprint arXiv:2502.17105*, 2025.

[15] J. Han, J. Liu, Y. Jiang, B. Yan, Y. Zhang, Z. Yuan, B. Peng, and X. Liu. Infinity: Scaling bitwise autoregressive modeling for high-resolution image synthesis. *arXiv preprint arXiv:2412.04431*, 2024.

[16] J. Ho et al. Denoising diffusion probabilistic models. *Advances in Neural Information Processing Systems*, 33:6840–6851, 2020.

[17] D. Karageorgiou, S. Papadopoulos, I. Kompatsiaris, and E. Gavves. Any-resolution ai-generated image detection by spectral learning. In *CVPR*, 2025.

[18] T. Karras et al. Progressive growing of gans for improved quality, stability, and variation. In *International Conference on Learning Representations*, 2018.

[19] T. Karras et al. A style-based generator architecture for generative adversarial networks. In *Proceedings of the IEEE/CVF Conference on Computer Vision and Pattern Recognition*, pages 4401–4410, 2019.

[20] B. F. Labs. Flux. `https://github.com/black-forest-labs/flux`, 2024.

[21] O. Li, J. Cai, Y. Hao, X. Jiang, Y. Hu, and F. Feng. Improving synthetic image detection towards generalization: An image transformation perspective. *arXiv preprint arXiv:2408.06741*, 2024.

[22] T.-Y. Lin et al. Microsoft coco: Common objects in context. In *European Conference on Computer Vision*, pages 740–755. Springer, 2014.

[23] T.-Y. Lin, M. Maire, S. Belongie, J. Hays, P. Perona, D. Ramanan, P. Dollár, and C. L. Zitnick. Microsoft coco: Common objects in context. In *Computer vision–ECCV 2014: 13th European conference, zurich, Switzerland, September 6-12, 2014, proceedings, part v 13*, pages 740–755. Springer, 2014.

[24] H. Liu et al. Spatial-phase shallow learning: rethinking face forgery detection in frequency domain. In *Proceedings of the IEEE/CVF Conference on Computer Vision and Pattern Recognition*, pages 772–781, 2021.

[25] H. Liu, Z. Tan, C. Tan, Y. Wei, J. Wang, and Y. Zhao. Forgery-aware adaptive transformer for generalizable synthetic image detection. In *Proceedings of the IEEE/CVF Conference on Computer Vision and Pattern Recognition*, pages 10770–10780, 2024.

[26] U. Ojha et al. Towards universal fake image detectors that generalize across generative models. In *Proceedings of the IEEE/CVF Conference on Computer Vision and Pattern Recognition*, pages 24480–24489, 2023.

[27] A. S. Rajan, U. Ojha, J. Schloesser, and Y. J. Lee. Aligned datasets improve detection of latent diffusion-generated images, 2025.

[28] R. Rombach et al. High-resolution image synthesis with latent diffusion models. In *Proceedings of the IEEE/CVF Conference on Computer Vision and Pattern Recognition*, pages 10684–10695, 2022.

[29] Z. Sha, Z. Li, N. Yu, and Y. Zhang. De-fake: Detection and attribution of fake images generated by text-to-image generation models. In *Proceedings of the 2023 ACM SIGSAC conference on computer and communications security*, pages 3418–3432, 2023.

[30] C. Tan et al. Learning on gradients: Generalized artifacts representation for gan-generated images detection. In *Proceedings of the IEEE/CVF Conference on Computer Vision and Pattern Recognition (CVPR)*, pages 12105–12114, June 2023.

[31] C. Tan, R. Tao, H. Liu, G. Gu, B. Wu, Y. Zhao, and Y. Wei. C2p-clip: Injecting category common prompt in clip to enhance generalization in deepfake detection. In *Proceedings of the AAAI Conference on Artificial Intelligence*, 2024.

[32] C. Tan, Y. Zhao, S. Wei, G. Gu, P. Liu, and Y. Wei. Frequency-aware deepfake detection: Improving generalizability through frequency space domain learning. In *Proceedings of the AAAI Conference on Artificial Intelligence*, volume 38, pages 5052–5060, 2024.

[33] C. Tan, Y. Zhao, S. Wei, G. Gu, P. Liu, and Y. Wei. Rethinking the up-sampling operations in cnn-based generative network for generalizable deepfake detection. In *Proceedings of the IEEE/CVF Conference on Computer Vision and Pattern Recognition*, pages 28130–28139, 2024.

[34] S.-Y. Wang et al. Cnn-generated images are surprisingly easy to spot... for now. In *Proceedings of the IEEE/CVF Conference on Computer Vision and Pattern Recognition*, pages 8695–8704, 2020.

[35] S. Xiao, Y. Wang, J. Zhou, H. Yuan, X. Xing, R. Yan, C. Li, S. Wang, T. Huang, and Z. Liu. Omnigen: Unified image generation. *arXiv preprint arXiv:2409.11340*, 2024.

[36] S. Yan, O. Li, J. Cai, Y. Hao, X. Jiang, Y. Hu, and W. Xie. A sanity check for ai-generated image detection. *arXiv preprint arXiv:2406.19435*, 2024.

[37] Z. Yan, T. Yao, S. Chen, Y. Zhao, X. Fu, J. Zhu, D. Luo, C. Wang, S. Ding, Y. Wu, et al. Df40: Toward next-generation deepfake detection. *arXiv preprint arXiv:2406.13495*, 2024.

[38] Z. Yan, J. Ye, W. Li, Z. Huang, S. Yuan, X. He, K. Lin, J. He, C. He, and L. Yuan. Gpt-imgeval: A comprehensive benchmark for diagnosing gpt4o in image generation. *arXiv preprint arXiv:2504.02782*, 2025.

[39] X. Yu, K. Chen, K. Zeng, H. Fang, Z. Yang, X. Shang, Y. Qi, W. Zhang, and N. Yu. Semgir: Semantic-guided image regeneration based method for ai-generated image detection and attribution. In *Proceedings of the 32nd ACM International Conference on Multimedia*, pages 8480–8488, 2024.

[40] Y. Zhang, Y. Wei, D. Jiang, X. Zhang, W. Zuo, and Q. Tian. Controlvideo: Training-free controllable text-to-video generation. *arXiv preprint arXiv:2305.13077*, 2023.

[41] C. Zheng, C. Lin, Z. Zhao, H. Wang, X. Guo, S. Liu, and C. Shen. Breaking semantic artifacts for generalized ai-generated image detection. *Advances in Neural Information Processing Systems*, 37:59570–59596, 2024.

[42] M. Zhu, H. Chen, Q. Yan, X. Huang, G. Lin, W. Li, Z. Tu, H. Hu, J. Hu, and Y. Wang. Genimage: A million-scale benchmark for detecting ai-generated image. *Advances in Neural Information Processing Systems*, 36:77771–77782, 2023.